separations

MDPI

Article

Separation of Zinc from Zinc Ferrite by Magnetization Roasting and Ammonia Leaching

Zeqiang Xie, Tao Jiang, Yufeng Guo *, Shuai Wang, Feng Chen, Lingzhi Yang and Ganghua Fu *

School of Minerals Processing and Bioengineering, Central South University, Changsha 410083, China; zeqiangxie@csu.edu.cn (Z.X.); jiangtao@csu.edu.cn (T.J.); wang_shuai@csu.edu.cn (S.W.); csuchenf@csu.edu.cn (F.C.); yanglingzhi@csu.edu.cn (L.Y.)

* Correspondence: yfguo@csu.edu.cn (Y.G.); fugh@csu.edu.cn (G.F.); Tel.: +86-0731-88830346 (Y.G.)

Abstract: Zinc ferrite can be found in zinc-bearing dust in ironmaking and steelmaking. It is difficult to be recovered due to its stable properties. The magnetization roasting and ammonia leaching method were used to separate iron and zinc from zinc ferrite in this study. Thermodynamic analysis showed that the key to the selective reduction of zinc ferrite to zinc oxide and ferric oxide is to control the appropriate temperature and atmosphere. The influences of the selective reduction roasting process of zinc ferrite on the conversion rate, phase change, and microevolution behavior were investigated. The microstructure analysis showed that the distribution area of iron was mainly gray, and the distribution area of zinc was mainly white grid lines. The zinc content in the white area was higher than that in the gray area. With the increase in temperature and P_{CO}, the white area expanded and the migration of zinc and iron was accelerated, but the iron in the white area still existed. The ammonia leaching of the magnetization-roasted product showed that a zinc leaching rate of 78.12% was achieved under the following conditions: the roasting atmosphere of $P_{CO}/P_{(CO+CO2)}$ = 25%, the roasting temperature of 750 °C, roasting duration for 45 min, n(NH_3-H_2O):n(NH_4Cl) = 1:1, the solid–liquid ratio of 40 g/L, leachate concentration of 6 mol/L, leaching duration of 90 min, the leaching temperature of 50 °C, and the stirring rate of 200 rpm.

Keywords: zinc ferrite; magnetization roasting; microstructure; zinc oxide; ammonia leaching; strategic minerals

check for updates

Citation: Xie, Z.; Jiang, T.; Guo, Y.; Wang, S.; Chen, F.; Yang, L.; Fu, G. Separation of Zinc from Zinc Ferrite by Magnetization Roasting and Ammonia Leaching. *Separations* **2023**, *10*, 299. https://doi.org/10.3390/separations10050299

Academic Editor: Guoquan Zhang

Received: 31 March 2023
Revised: 26 April 2023
Accepted: 6 May 2023
Published: 8 May 2023

Copyright: © 2023 by the authors. Licensee MDPI, Basel, Switzerland. This article is an open access article distributed under the terms and conditions of the Creative Commons Attribution (CC BY) license (https://creativecommons.org/licenses/by/4.0/).

1. Introduction

Zinc is one of the important strategic metals [1]. With the acceleration of the world's modernization, zinc-bearing productions are increasingly unable to meet the consumption demand, and the shortage of zinc resources will seriously affect the economy and security [1,2]. It is important to increase technological development for the efficient zinc recycling from zinc ore resources and zinc-containing secondary resources. In China, with the increasing capacity of zinc resources, the zinc leach residue is roughly 5 million tons per year, which contains 20% zinc; however, the zinc utilization rate is low [3]. Moreover, roughly 100 million tons of dust are formed in steel plants each year, and the utilization rate for this is less than 20% [4]. China currently produces many zinc-containing secondary resources with high-content zinc resources. However, because zinc in such resources exists in the form of zinc ferrite phase [5], the processing is relatively difficult; although it belongs to the bulk of the secondary zinc resources, the recovery rate is very low.

Zinc ferrite is a spinel structure with very stable physicochemical properties, making it difficult to choose common hydrometallurgical methods and routes for recycling, while the presence of large amounts of valuable metals mixed into the zinc ferrite lattice can have a large impact on the recycling of iron resources as well as other valued metals [6]. The current treatment of electric furnace dust in steel plants is based on recycling, including hydro- and pyrometallurgical treatment methods and other hydro- and pyrometallurgical synergistic treatment technologies that are not promoted for industrial application [4,7–11].

The direct recycling of zinc-containing dust in steel companies is achieved by using electric furnace dust in the sintering process and recycling the iron resources in an integrated way [12–14]. However, the dust is usually of very fine particle size, and, therefore, the permeability of the sintering layer is affected. Furthermore, as blast furnace smelting limits the zinc content of the charge to a certain extent, the zinc content of the sintered or pellet-treated zinc-containing dust must, therefore, not be too high [4,15]. In addition, one of the common methods of treating secondary resources is the acid-leaching method [16–18]. In the acid leaching process, the soluble zinc phases in the dust are dissolved in the acid and incorporated into the leaching solution, such as zinc oxide, after which the leaching solution is purified and then treated by electrowinning to obtain metallic zinc ingots, enabling the comprehensive recycling of zinc resources in this way [19,20]. Dimitrios Filippou [21] studied the reaction kinetics of zinc ferrite particles with different acid concentrations (0.25–1.5 M). The highest conversion of zinc ferrite was achieved with 1 M H_2SO_4 at 368 K after 240 min of leaching time [21]. Moreover, alkali leaching mainly involves the application of alkaline solutions, such as sodium hydroxide, in the leaching process of electric furnace dust, by which valuable metal elements are obtained [22]. Compared to acid leaching, this method is non-corrosive to the production plant and has a better selective leaching effect. However, the leaching rate of this method is also not very high. Dutra [23] and Orhan et al. [24] obtained 74% and 85% Zn recovery, respectively, by conventional alkaline leaching experiments and suggested that the insolubility of $ZnFe_2O_4$ in the dust was the main reason for the low leaching rate. Due to the low aqueous solubility of zinc ferrite, most of the hydrometallurgical processes are not economically feasible for the extraction of zinc or iron as zinc residues typically contain only 15–20% of zinc and iron [25].

For the pyrometallurgy processes, the representative processes for the treatment of zinc-containing dust by direct reduction include rotary hearth furnaces, rotary kilns, and circulating fluidized bed processes. The rotary kiln technology is matured and the production plant is large-scale; however, the technology has disadvantages, such as high energy consumption, high production plant costs, and deposit formation in kilns. The melting reduction method can obtain a higher quality of iron and a higher dezincification rate; however, the method has its drawbacks, such as high energy consumption and high treatment costs [9]. More and more experts and scholars are beginning to study the roasting conversion of zinc ferrite followed by the recycling of zinc and iron resources [26–28]. Some researchers treated zinc-containing electric furnace dust by applying the magnetization roasting–magnetic separation method [15,29]. Han et al. [30] achieved a zinc recovery of 92.6% by reduction roasting with acid leaching, while the iron remained in the slag and could be recovered from the residue after magnetic separation. Most zinc-bearing secondary resources contain zinc in the form of zinc ferrite, which is more stable and more difficult to extract from zinc and iron. The design and development of a more efficient and less polluting recycling process technology for secondary zinc resources will not only generate greater economic benefits but will also ensure higher environmental benefits, helping to solve the structural contradictions of zinc resources as well as being an important way to promote the rapid development of the economy.

This study investigated the effects of the roasting atmosphere and temperature on the phase transformation of zinc ferrite and microstructures of the roasted samples. The XRD and SEM-EDS techniques were used to determine the phases and microstructure of samples. Moreover, the verified ammonia leaching test of the magnetization roasting products was carried out. This study will provide the technical basis for the high efficient utilization of zinc-ferrite-containing resources.

2. Materials and Methods

2.1. Raw Materials

The chemical reagents used in this study were bought from Shanghai Macklin Biochemical Technology Co., Ltd. (Shanghai, China). The used zinc ferrite in this study was produced by sintering of ZnO and Fe_2O_3. The analyzed pure ZnO and Fe_2O_3 were thor-

oughly mixed in a planetary ball mill according to the molar ratio of 1:1. The mixture was put into a 200 mL corundum crucible and then placed into a muffle furnace and heated at 1200 °C for 4 h. After taking out the sample and cooling, the sample was ground to less than 0.074 mm by a ball mill. Further, 1 mol/L hydrochloric acid solution was used for stirring leaching for 1 h at room temperature to remove the unreacted ZnO and Fe_2O_3. After drying, the samples were roasted at 1200 °C for 1 h. After cooling, the samples were taken out and ground to less than 0.074 mm and stored in the dryer for later use.

The XRD patterns of zinc ferrite are shown in our previous paper [31]. The content of zinc and iron in the synthesized zinc ferrite was 26.94% and 46.61%, respectively, which was very close to the theoretical content of 27.12% and 46.33% [31]. It is proven that the synthesized zinc ferrite was pure.

2.2. Experimental Equipment and Methods

The magnetization roasting of zinc ferrite samples was conducted in a vertical tube furnace (HF-KEJING, Hefei, China), which was heated by a silicon carbon rod and equipped with an automatic temperature control system, as shown in Figure 1. The pressed zinc ferrite pellets were evenly dispersed into a quartz tube fitted with a slotted gasket with an internal diameter of 54 mm. The number of pellets was 10 (2.5 g each). Firstly, N_2 gas was passed to drive the air out of the furnace. When the reduction shaft furnace raised to the roasting temperature and the temperature was stable, we quickly put the quartz tube into the reduction shaft furnace and adjusted the flow rate of CO, CO_2, and N_2 according to the preset ratio. After the setting time of constant temperature roasting, we stopped passing CO and CO_2 and took the quartz tube out of the reduction shaft furnace under the protection of high-purity N_2 gas. After cooling to room temperature, the samples were taken out and the roasted samples were ground to less than 0.074 mm for the content detection of Zn and Fe elements and the analysis of phase. The leaching method of the samples was also described in our previous paper [31]. The leaching experiments were conducted in a 250 mL beaker heated in a water bath. The leaching procedure was initiated by pouring 100 mL of the required concentration of ammonia leaching agent into a 250 mL beaker. After the required leaching duration ended, the leachate was separated from the residue by vacuum filtration and analyzed. Figure 2 shows the comparison before and after roasting of pure zinc ferrite after being pressed together. Before roasting, zinc ferrite was red, and zinc ferrite was transformed into black after roasting.

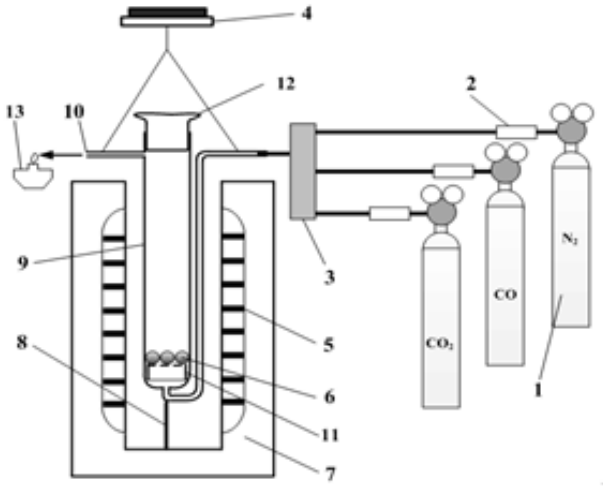


Figure 1. Schematic diagram of a vertical reducing furnace. 1—Gas tank; 2—Gas flowmeter; 3—Gas mixer; 4—Lifter; 5—Heating element; 6—Sample; 7—Shaft furnace; 8—Thermocouple; 9—Quartz tube; 10—Air outlet; 11—Perforated plate; 12—Quartz cover; 13—Alcohol lamp.

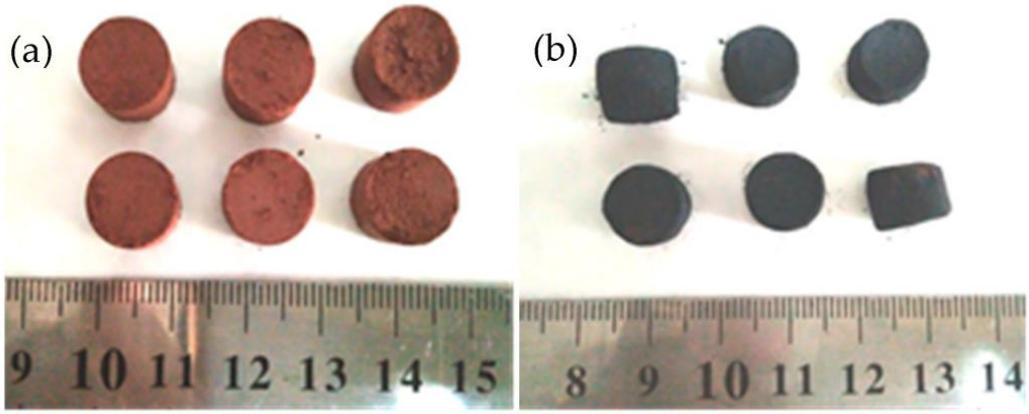


Figure 2. Comparison of zinc ferrite before and after magnetization roasting: (**a**) before roasting; (**b**) after roasting.

2.3. Analysis Methods

The zinc content of samples was determined by the EDTA complexometric titration (GB/T 8151.1-2012). The total iron was determined by GB/T 6730.5-2022 (titrimetric methods after titanium (III) chloride reduction). The Fe^{2+} was analyzed by GB/T 6730.8-2016 (potassium dichromate titrimetric method). The phase compositions of samples were analyzed by X-ray diffraction (Rigaku-TTRJII, Cu target, Kα,γ = 0.15406 nm). The microstructure of the magnetized calcined zinc ferrite was observed by a microscope after a series of treatments, including gluing, cold setting, grinding, and polishing. The microstructure and elemental distributions of the samples were determined by SEM (TESCAN, MIRA3-LMH, Czech) with EDS (Oxford X-MAX20). The relative deviation is 5% for elements with content higher than 20%, 10% for those with 3–20%, 20% for those with 1–3%, and 50% for those with 1% or less.

3. Results and Discussion

3.1. Thermodynamic Analysis of the Magnetized Roasted Process of Zinc Ferrite

The reduction roasting of zinc ferrite was carried out in a non-standard state and the composition of the reduction products was related to the roasting atmosphere, roasting temperature, etc. Figure 3 shows a map of the dominant region of Fe-Zn-O at different temperatures and various $P_{CO}/P_{(CO+CO2)}$ as calculated by FactSage 8.0 software. The reduction conditions for the reduction of Zn-Fe-O to ZnO and Fe_3O_4 can be tentatively determined from Figure 3. The yellow area in Figure 3 is a map of the dominant region for the selective reduction of zinc ferrite to ZnO and Fe_3O_4. Overall, the $P_{CO}/P_{(CO+CO2)}$ dominant region for the selective reduction of zinc ferrite to ZnO and Fe_3O_4 increases gradually with increasing temperatures below 560 °C. Above 560 °C, the $P_{CO}/P_{(CO+CO2)}$ dominance region for the selective reduction of zinc ferrite to ZnO and Fe_3O_4 gradually decreases with the increasing temperature. At temperatures above 930 °C, the reduced zinc oxide is over-reduced to zinc metal vapor. In the temperature range of 400–1100 °C, the stable presence of $P_{CO}/P_{(CO+CO2)}$ of zinc ferrite is maintained at a very low level of less than 2%.

3.2. Effect of Temperature on Phase Transformation

The effects of temperature on the phase composition of the roasted samples were analyzed. The roasting conditions were as follows: total gas flow rate of 8 L/min, with 40% of the total partial pressure of carbon monoxide and carbon dioxide, roasting time of 1 h, and $P_{CO}/P_{(CO+CO2)}$ = 25% was fixed. The crystal structures of Fe_3O_4 and $ZnFe_2O_4$ are similar and the characteristic peaks of the two substances on the XRD patterns are very close. In this study, XRD slow scan analysis of the $ZnFe_2O_4$ reduction products was carried

out at a 2θ angle in the range of 60–65° to analyze the change in the phase of the $ZnFe_2O_4$ reduction process. Figure 4 shows the XRD patterns of the reduction-roasted products.

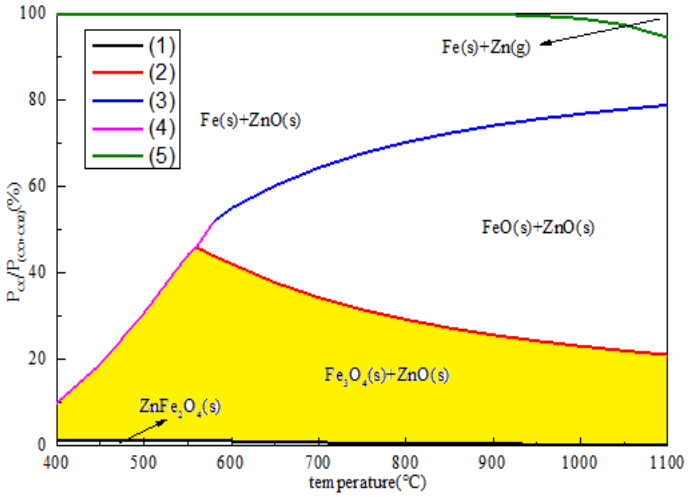


Figure 3. The selective reduction of zinc ferrite dominant area at 400–1100 °C.

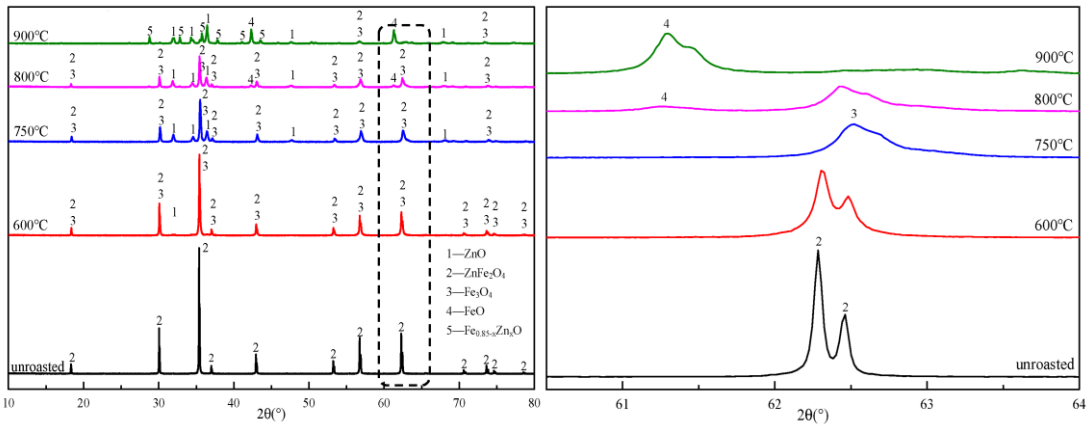


Figure 4. XRD patterns of magnetization-roasted products at different roasting temperatures.

The roasting temperature has an important effect on the selective reduction of zinc ferrite. A small diffraction peak of zinc oxide can be observed at 600 °C, but the slow scanning results show that the peaks of $ZnFe_2O_4$ do not shift significantly, which indicates that the reaction is slow at a lower temperature and the contents of ZnO and Fe_3O_4 are low. With the increase in temperature, the diffraction peaks of ZnO are enhanced, indicating that the zinc oxide is increased. The characteristic peaks of $ZnFe_2O_4$ move towards the characteristic peaks of Fe_3O_4 when the roasting temperature is 750 °C. At 800 °C, the characteristic peaks of ZnO decrease, indicating that ZnO in the product is reduced. The XRD pattern also shows the characteristic peaks of FeO, which also indicates the presence of FeO due to the over-reduction of zinc ferrite. The characteristic peaks of $ZnFe_2O_4$ move up to that of Fe_3O_4. To prevent the over-reduction of $ZnFe_2O_4$ and the formation of FeO, the roasting temperature should be controlled below 800 °C. At 900 °C, the diffraction peaks of zinc–iron solid solution ($Fe_{0.85-x}Zn_xO$) appear, while the diffraction peaks of ZnO continue to weaken, and the characteristic peaks of iron oxide are significantly enhanced. According to the above analysis, the phase change of zinc ferrite during the magnetization roasting process is significantly affected by the roasting temperature. At higher roasting temperatures, zinc ferrite is easy to be over-reduced and zinc oxide content is reduced, so the magnetization roasting process of zinc ferrite should not exceed 800 °C.

3.3. Effects of Temperature and Reduction Potential on the Conversion of Zinc Oxide

The conversion percentage of zinc ferrite to zinc oxide in the magnetization roasting process was studied in this section. A higher conversion rate could provide a basis for the subsequent separation of zinc and iron. The influence of roasting temperature under different reducing atmospheres on the conversion rate of zinc oxide was analyzed. The optimum conversion rate could be obtained under the roasting system.

As shown in Figure 5, when $P_{CO}/P_{(CO+CO2)}$ is 5%, the conversion rates are 30.9% at 700 °C and 60.2% at 900 °C; the conversion rate of zinc oxide increases with the increase in temperature. However, when the temperature reaches 900 °C, the conversion rate of zinc oxide is still not high.

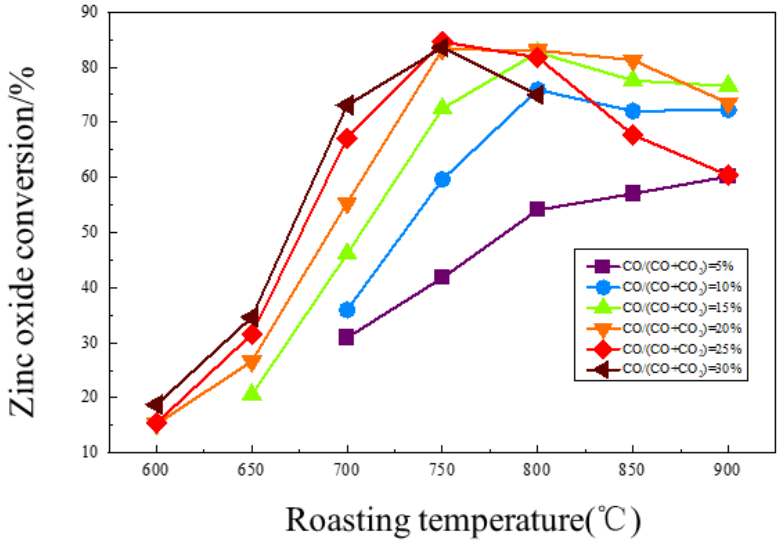


Figure 5. Relationship between zinc oxide conversion and temperature under different roasting atmospheres.

When the magnetization roasting atmosphere is 10% and $P_{(CO+CO2)}$ is 10%, ZnO conversion reaches the maximum of 75.9% at 800 °C, while zinc oxide conversion decreases as the temperature continues to rise. Phase analysis shows that, when the roasting temperature exceeds 800 °C, the solid solution phase of ferrous oxide and zinc–iron appears in the roasting product, resulting in the decrease in zinc oxide content, so the roasting temperature should not be too high. Furthermore, the ZnO conversion reaches the maximum of 82.7% at 800 °C when $P_{CO}/P_{(CO+CO2)}$ = 15% and decreases with the increase in temperature. This pattern is similar to that of $P_{CO}/P_{(CO+CO2)}$ = 10%. The reason is the over-reduction of zinc ferrite after 800 °C. The maximum zinc oxide conversion rate reaches 83.2% at 750 °C under 20% $P_{CO}/P_{(CO+CO2)}$ and decreases with the increase in roasting temperature. The optimum roasting temperature is lower than 750 °C at a roasting atmosphere of 20% $P_{CO}/P_{(CO+CO2)}$.

The conversion of zinc oxide is similar to that of $P_{CO}/P_{(CO+CO2)}$ = 20% in a magnetization roasting atmosphere of 25% P_{CO}. When the roasting temperature is below 750 °C, the zinc oxide conversion reaches the highest point, 85.31% at 750 °C, but decreases with the increase in roasting temperature, and the zinc conversion drops to 56.79% at 900 °C. This is due to the increase in zinc–iron solid solution produced by reduction at high temperatures. When the magnetization roasting atmosphere of $P_{CO}/P_{(CO+CO2)}$ is 30%, the maximum ZnO conversion rate reaches 83.58% at 750 °C. However, if the temperature continues to rise, the conversion rate decreases.

When $P_{CO}/P_{(CO+CO2)}$ is 5%, the conversion of zinc oxide is generally low. With the enhancement of roasting and reduction atmosphere, the conversion rate of zinc oxide increases but reaches the highest value at 750–800 °C. With the continuous increase in temperature, the conversion rate decreases slightly because the over-reduction of zinc ferrite occurred under the stronger roasting atmosphere and higher temperature conditions,

and the conversion rate of zinc oxide is reduced. In conclusion, the optimum roasting conditions are as follows: $P_{CO}/P_{(CO+CO2)}$ = 25%, the roasting temperature is 750 °C, the roasting time is 60 min, and the conversion rate of zinc oxide is 85.3%.

3.4. Effects of Temperature and Potential on the Decomposition Rate of Zinc Ferrite

Since zinc ferrite cannot be reduced to metal iron under the above conditions and the valence state of iron in zinc ferrite would only be reduced to Fe^{2+}, Fe^{2+}/TFe is, therefore, chosen to reflect the decomposition rate of zinc ferrite. If the reduction product of zinc ferrite is Fe_3O_4, Fe^{2+}/TFe = 33.3%; if there is some zinc ferrite not reduced, Fe^{2+}/TFe is less than 33.3%; if there is FeO in the reduction product, Fe^{2+}/TFe exceeds 33.3%. Therefore, the degree of reducing zinc ferrite can be determined by the results of Fe^{2+}/TFe.

The effects of roasting temperature and reduction potential on the decomposition rate of zinc ferrite were studied under the roasting time of 60 min and the total pressure of fixed gas was 8 L/min, in which N_2 accounted for 60% and $CO+CO_2$ accounted for 40%. See Figure 6 for the results.

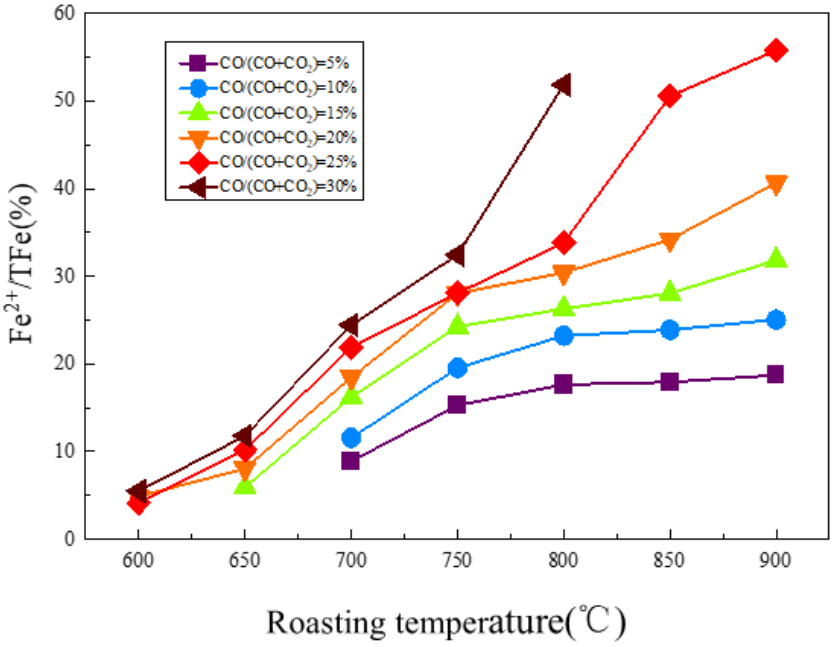


Figure 6. Effects of roasting temperature and $P_{CO}/P_{(CO+CO2)}$ on the ratio of Fe^{2+}/TFe of samples.

The Fe^{2+}/TFe ratio is only 8.9% at 700 °C with $P_{CO}/P_{(CO+CO2)}$ = 5% and increases slightly with the increase in temperature, 18.7% at 900 °C. However, it is still far less than 33.33%, which also indicates that zinc ferrite is not fully converted. The Fe^{2+}/TFe ratio is higher than that of $P_{CO}/P_{(CO+CO2)}$ = 5% at the same temperature in a roasting atmosphere of 10%. The decomposition rate of zinc ferrite increases with increasing roasting temperature. At 700 °C, the Fe^{2+}/TFe ratio is 11.6%, and, at 900 °C, the Fe^{2+}/TFe ratio is 25.0%, which is still smaller than 33.33%, indicating that the zinc ferrite could not be selectively reduced completely under the above roasting conditions. The Fe^{2+}/TFe of the roasted products increases with the increase in temperature when $P_{CO}/P_{(CO+CO2)}$ = 15% is used. When the roasting temperature is 650 °C, the Fe^{2+}/TFe of the product is only 5.94%. When the roasting temperature is 900 °C, the ratio is 31.84%, which is close to the theoretical Fe^{2+}/TFe ratio of 33.33%. The selective reduction of zinc ferrite is almost complete. When $P_{CO}/P_{(CO+CO2)}$ = 20%, the decomposition rate of zinc ferrite increases with the increase in roasting temperature. At 850 °C, the percentage of Fe^{2+}/TFe is 34.2%, higher than 33.33%, indicating the excessive reduction of zinc ferrite under the above roasting conditions. Under the roasting atmosphere of 25% $P_{CO}/P_{(CO+CO2)}$, Fe^{2+}/TFe is 33.83% at 800 °C, which is slightly higher than 33.33%. When combined with the actual ZnO conversion, zinc ferrite

is over-reduced at 800 °C. When $P_{CO}/P_{(CO+CO2)}$ is 30% at 800 °C, the ratio of Fe^{2+}/TFe reaches 51.85%, much higher than 33.33%, indicating that the degree of over-reduction of zinc ferrite is greater.

In conclusion, according to the comparison between the conversion rate of zinc oxide and the decomposition rate of zinc ferrite, it can be found that the selective reduction of zinc ferrite can be characterized by Fe^{2+}/TFe, but it cannot fully reflect the actual situation. In the actual reaction process, the conversion rate of zinc oxide decreases due to the zinc–iron solid solution produced by the over-reduction of zinc ferrite, thus affecting the recovery of zinc oxide. In general, the roasting temperature has an important effect on the selective reduction of zinc ferrite.

3.5. Microstructure Analysis of Reduction Products

The microstructures of the products obtained at 600 °C, 750 °C, and 900 °C for 1 h with P_{CO} = 25% were studied by scanning electron microscopy (SEM). As shown in Figure 7, the microstructures of the products vary with different roasting temperatures. With the increase in temperature, the structure of zinc ferrite is damaged and zinc oxide was precipitated by reduction reactions. The migration is not obvious at a low temperature. When the temperature exceeds 750 °C, a grid structure appears, and the grid lines are the migrated zinc oxide. As shown in Figure 7, zinc ferrite particles present different reduction states under different roasting temperatures. With the increase in roasting temperature, the reduction degree of zinc ferrite is deepened, and the zinc oxide gradually migrates from the zinc ferrite. When the roasting temperature is 600 °C, the reaction rate is slow, the reduction degree of zinc ferrite particles is low, and the zinc migration is not obvious, but a grid zinc migration pathway has appeared. At 750 °C, the white grid is obvious, and most of the zinc has migrated out. At 900 °C, a new phase appears. According to the analysis of the composite phase, ferrous appears in the darker-color area and the grid white area is more concentrated, indicating deeper zinc migration.

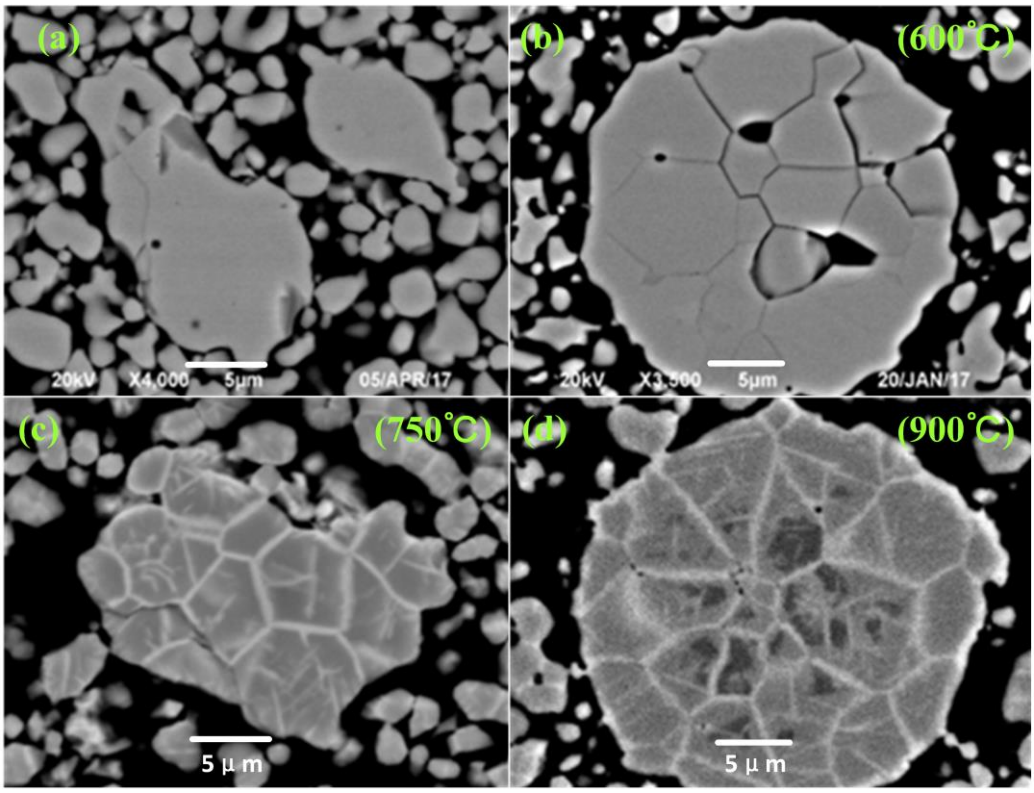


Figure 7. The microstructure under different roasting temperatures: (**a**) synthesis of zinc ferrite; (**b**) 600 °C; (**c**) 750 °C; (**d**) 900 °C.

According to Figures 8 and 9, it can be found that the distribution area of iron is mainly gray and the distribution area of zinc is mainly white grid lines, indicating that zinc and iron gradually separate and migrate in the reduction process of zinc ferrite. The zinc content in the white area is higher than that in the gray area. However, there is still some iron in the white area, which indicates that the separation of zinc and iron is not thorough enough. With the increase in temperature, the white area expands and the migration of zinc and iron is accelerated, but the iron in the white area still exists because the roasting time is only one hour; it is difficult to realize the complete migration and separation of zinc and iron under the limited time.

Figure 10 shows the SEM images of the roasting products at 750 °C for $P_{CO}/P_{(CO+CO2)}$ = 5%, 25%, and 35%. The microstructure of the products differs for various $P_{CO}/P_{(CO+CO2)}$. As the $P_{CO}/P_{(CO+CO2)}$ increases, the structure of zinc ferrite appears to break down and zinc oxide precipitates reductively; the migration is not obvious at lower CO percentages. When the CO proportion exceeds $P_{CO}/P_{(CO+CO2)}$ = 25%, a clear lattice-like structure appears, and the grid lines are the reduced migrated zinc oxide. As the temperature continues to increase, at $P_{CO}/P_{(CO+CO2)}$ = 35%, a dark ferrous oxide phase appears.

3.6. Elemental Migration Behavior

Under the same roasting conditions as above, the elemental migration behavior of the magnetization products at 600 °C, 750 °C, and 900 °C was investigated using line scan energy spectroscopy, as shown in Figure 11.

The zinc and iron elements were evenly distributed at 600 °C, which can be explained regarding that, when the temperature was relatively low, the reduction reaction of zinc ferrite was slow, the reaction is not complete, the migration of elements is slow, and no obvious zinc aggregation yet occurred. When the roasting temperature raises to 750 °C, the zinc spectral lines in the white grid-like area show obvious peaks, with higher zinc content in the white line, mainly in the zinc oxide phase, while the iron spectral lines in the grey area also show obvious peaks, indicating the migration and aggregation of iron elements.

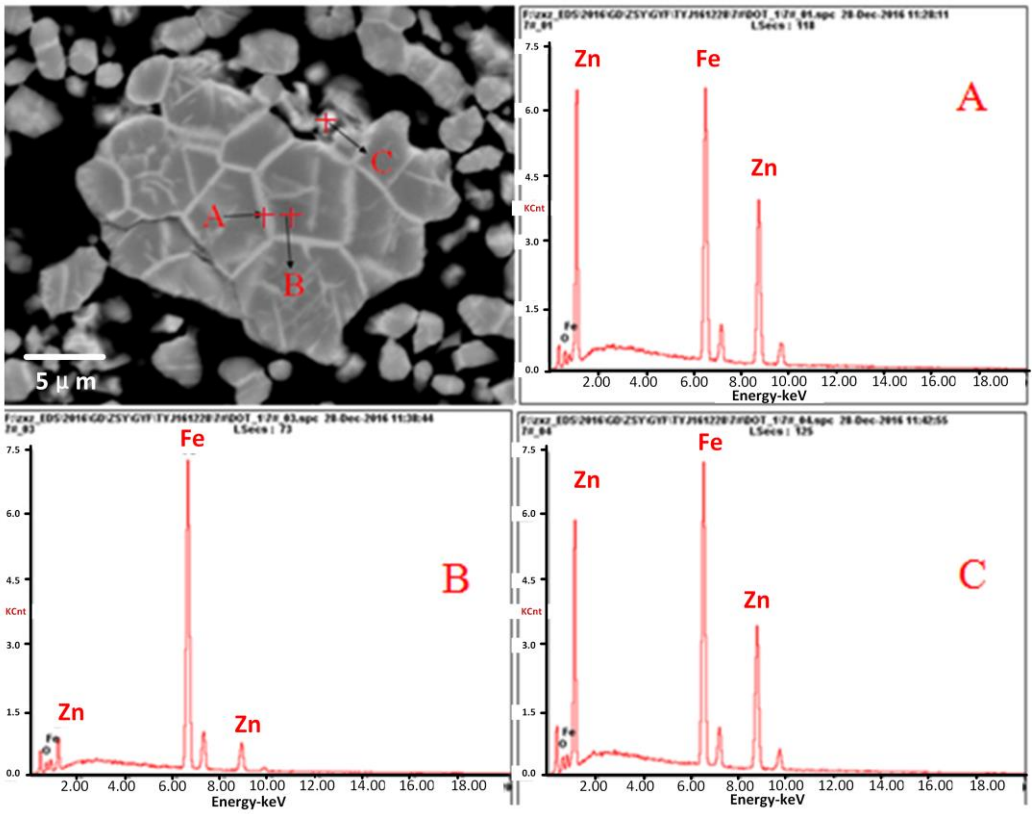


Figure 8. EDS of the roasted samples at 750 °C (points A, B, C and their related EDS analysis).

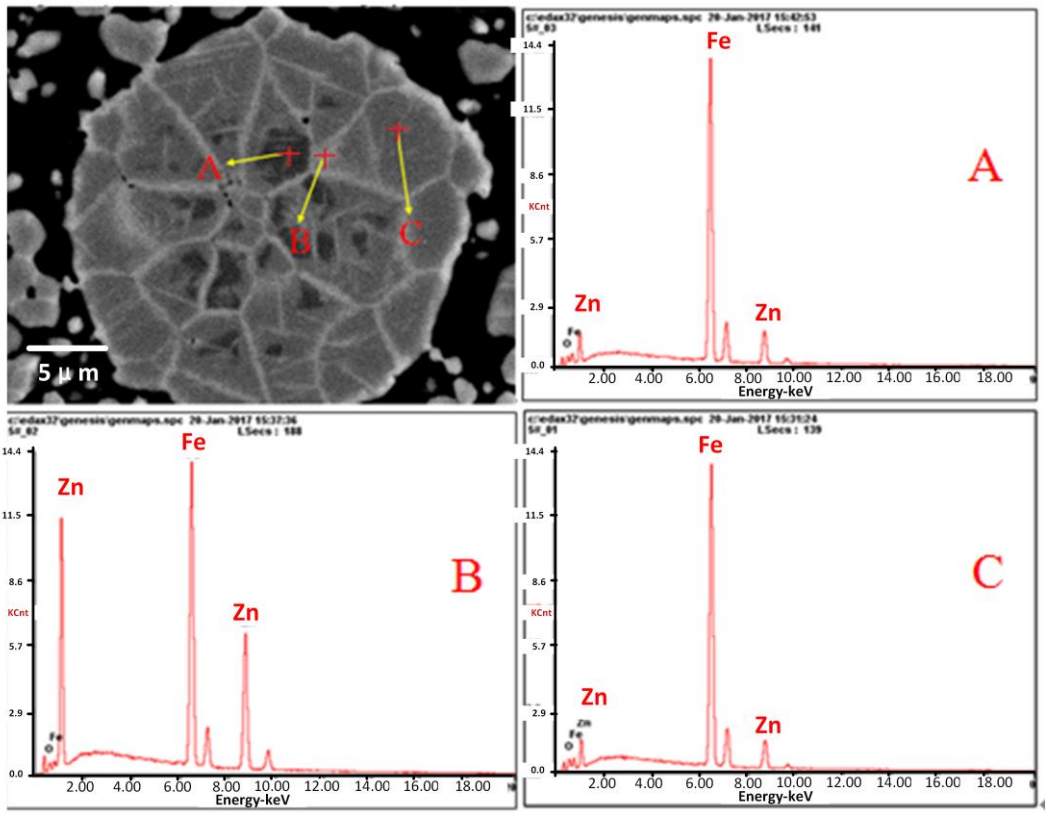


Figure 9. EDS of the roasted samples at 900 °C (points A, B, C and their related EDS analysis).

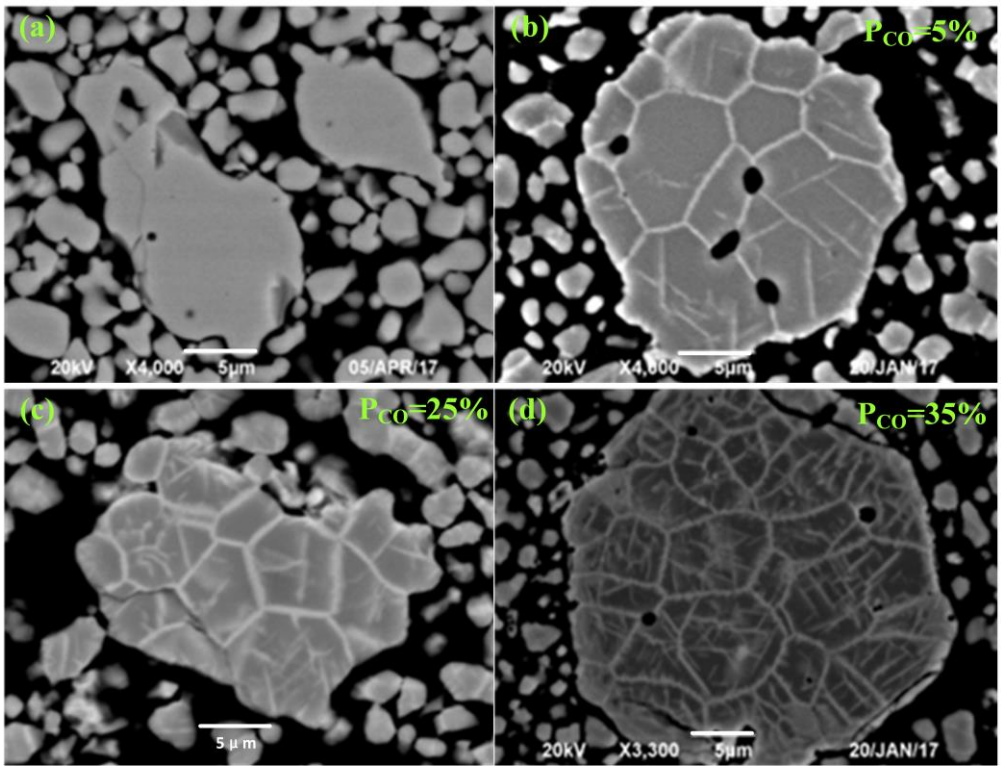


Figure 10. Microstructure of samples at various roasting atmospheres: (**a**) synthesis of zinc ferrite; (**b**) $P_{CO}/P_{(CO+CO2)}$ = 5%; (**c**) $P_{CO}/P_{(CO+CO2)}$ =25%; (**d**) $P_{CO}/P_{(CO+CO2)}$ = 35%.

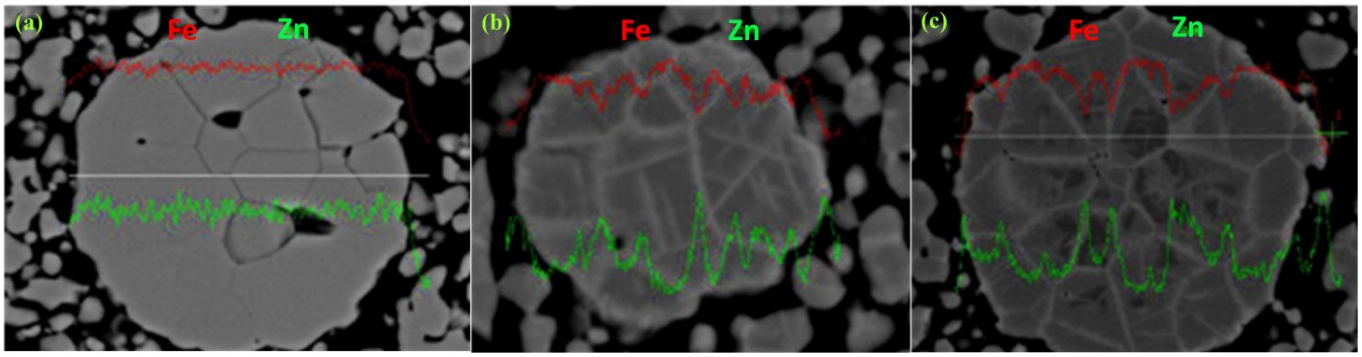


Figure 11. The line scanning of roasted products at different roasting temperatures: (**a**) 600 °C; (**b**) 750 °C; (**c**) 900 °C.

To analyze the migration behavior of Zn and Fe under different atmospheres, line scan analysis was performed for $P_{CO}/P_{(CO+CO2)}$ = 5%, 25%, and 35%. As shown in Figure 12, at $P_{CO}/P_{(CO+CO2)}$ = 5%, the zinc and iron are distributed more evenly, and there are no peaks and valleys of zinc and iron on the line scan spectra, which proves that the zinc and iron are distributed more evenly on the horizontal line. This phenomenon proves that, at $P_{CO}/P_{(CO+CO2)}$ = 5%, the reducing atmosphere is weak and the reduction reaction of zinc ferrite is weak too, so there is no significant migration of zinc elements. According to the line scan results at $P_{CO}/P_{(CO+CO2)}$ = 25%, there are distinct areas of white grids, which are randomly distributed throughout the particles. In combination with the line scan spectra, the zinc spectral lines in each white grid region of the line scan show distinct peaks, indicating higher zinc content in the white grid region. The Fe spectral line in the grey region also shows a clear peak, with the grey region inside the white grid having higher Fe content, indicating a gradual transition of elemental Zn from the grey region inside the white grid to the white region outside white grid. The line scan results at $P_{CO}/P_{(CO+CO2)}$ = 35% have more peaks for zinc and iron, demonstrating an increase in zinc and iron content in the line scan region, with zinc enriched in the white grid region and iron enriched in the grey region.

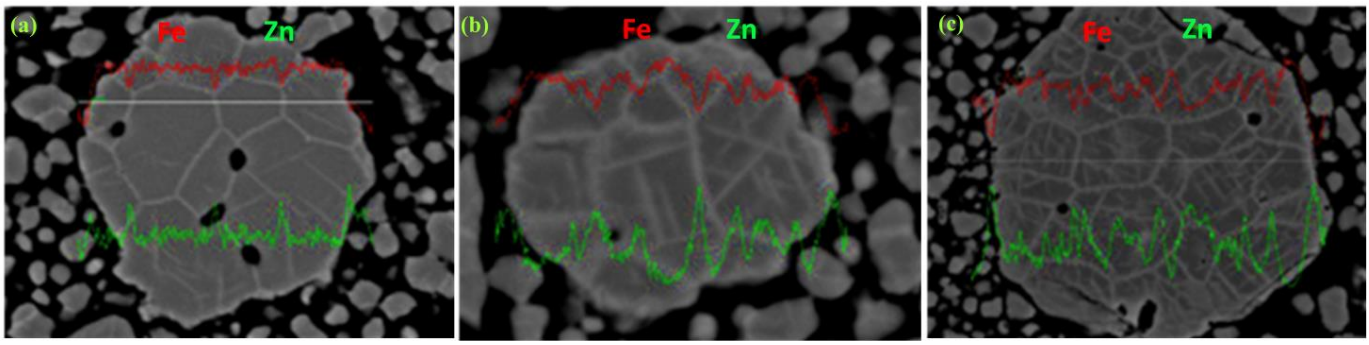


Figure 12. Line scanning under different roasting atmospheres: (**a**) $P_{CO}/P_{(CO+CO2)}$ = 5%; (**b**) $P_{CO}/P_{(CO+CO2)}$ = 25%; (**c**) $P_{CO}/P_{(CO+CO2)}$ = 35%.

3.7. Separation of Iron and Zinc from Reduced Samples by Ammonia Leaching

The main products of magnetization roasting of zinc ferrite are ZnO and Fe_3O_4. Because ZnO can form a complex with ammonia solution and enters the leaching solution while Fe_3O_4 cannot form a complex and then enters the leaching slag, the separation of zinc and iron from roasted products can be realized by the ammonia leaching method.

The optimal roasting conditions are as follows: $P_{CO}/P_{(CO+CO2)}$ = 25%, the roasting temperature of 750 °C, roasting time of 45 min, total gas pressure 8 L/min, 60% N_2, CO+CO_2 40%, and the partial gas pressure is determined by the composition of simulated blast furnace gas. The roasted zinc ferrite sample was ground to −0.074 mm and mixed evenly

as raw material. The leaching was carried out under the following optimum conditions: the ratio of ammonium chloride to ammonia was 1:1, the solid–liquid ratio was 40 g/L, the leaching temperature was 50 °C, the leachate concentration was 6 mol/L, the leaching duration was 90 min, and the stirring rate was 200 rpm. About a 78.12% zinc leaching rate was achieved.

4. Conclusions

The magnetization roasting temperature and atmosphere had great influences on the phase transformation of zinc ferrite. With the increase in temperature, the over-reduction of zinc ferrite was more likely to occur, generating FeO, metal iron, and metal zinc. The formed FeO easily formed a zinc–iron solid solution with ZnO, which harmed the zinc conversion rate. The phase reconstruction process of zinc ferrite in magnetization roasting should be controlled at the generation stage of Fe_3O_4 and ZnO. In the process of magnetization roasting of zinc ferrite, along with the transformation of zinc ferrite to Fe_3O_4 and ZnO, zinc ions in zinc ferrite migrate outward, forming a grid of zinc oxide minerals on the interface of new magnetite, embedded in the matrix of new formed magnetite grains. The magnetized zinc ferrite was obtained by roasting at 750 °C for 45 min under the roasting atmosphere of $P_{CO}/P_{(CO+CO2)}$ = 25%. Under the following conditions: the ratio of ammonium chloride to ammonia was 1:1, the solid–liquid ratio was 40 g/L, the leaching temperature was 50 °C, the leachate concentration of 6 mol/L was reached, the leaching duration was 90 min, and the stirring rate was 200 rpm, about a 78.12% zinc leaching rate was achieved.

Author Contributions: Methodology, Z.X.; software, S.W.; formal analysis, Z.X.; investigation, Z.X.; resources, T.J.; data curation, S.W.; writing—original draft preparation, Z.X.; writing—review and editing, S.W., G.F. and Y.G.; visualization, L.Y.; supervision, Y.G., G.F. and T.J.; project administration, F.C.; funding acquisition, Y.G. All authors have read and agreed to the published version of the manuscript.

Funding: This research was funded by the National Key Basic Research and Development Program (973 Program grant number 2014CB643403); Fundamental Research Funds for the Central Universities of Central South University, grant number 2018zzts221.

Data Availability Statement: Not application.

Conflicts of Interest: The authors declare no conflict of interest.

References

1. Pinc, J.; Kubasek, J.; Drahokoupil, J.; Capek, J.; Vojtech, D.; Skolakova, A. Microstructural and Mechanical Characterization of Newly Developed Zn-Mg-CaO Composite. *Materials* **2022**, *15*, 8703. [CrossRef] [PubMed]
2. Martynenko, N.; Anisimova, N.; Rybalchenko, O.; Kiselevskiy, M.; Rybalchenko, G.; Tabachkova, N.; Zheleznyi, M.; Temralieva, D.; Bazhenov, V.; Koltygin, A.; et al. Structure, Biodegradation, and In Vitro Bioactivity of Zn-1%Mg Alloy Strengthened by High-Pressure Torsion. *Materials* **2022**, *15*, 9073. [CrossRef] [PubMed]
3. Yujia, T.; Yufeng, G.; Tao, J.; Zeqiang, X.; Wei, C.; Xudong, L. Treatment technology and development of zinc electric arc furnace dust. *Multipurp. Util. Miner. Resour.* **2017**, *38*, 44–50.
4. Wang, J.; Zhang, Y.; Cui, K.; Fu, T.; Gao, J.; Hussain, S.; AlGarni, T.S. Pyrometallurgical recovery of zinc and valuable metals from electric arc furnace dust—A review. *J. Clean. Prod.* **2021**, *298*, 126788. [CrossRef]
5. Tang, H.; Peng, Z.; Wang, L.; Shang, W.; Anzulevich, A.; Rao, M.; Li, G. Facile synthesis of zinc ferrite as adsorbent from high-zinc electric arc furnace dust. *Powder Technol.* **2022**, *405*, 117479. [CrossRef]
6. Pickles, C.A. Thermodynamic modelling of the formation of zinc–manganese ferrite spinel in electric arc furnace dust. *J. Hazard. Mater.* **2010**, *179*, 309–317. [CrossRef]
7. Shawabkeh, R.A. Hydrometallurgical extraction of zinc from Jordanian electric arc furnace dust. *Hydrometallurgy* **2010**, *104*, 61–65. [CrossRef]
8. Zhang, H.; Li, J.; Xu, A.; Yang, Q.; He, D.; Tian, N. Carbothermic Reduction of Zinc and Iron Oxides in Electric Arc Furnace Dust. *J. Iron Steel Res. Int.* **2014**, *21*, 427–432. [CrossRef]
9. Li, C.; Liu, W.; Jiao, F.; Yang, C.; Li, G.; Liu, S.; Qin, W. Separation and recovery of zinc, lead and iron from electric arc furnace dust by low temperature smelting. *Sep. Purif. Technol.* **2023**, *312*, 123355. [CrossRef]
10. Stewart, D.J.C.; Barron, A.R. Pyrometallurgical removal of zinc from basic oxygen steelmaking dust—A review of best available technology. *Resour. Conserv. Recycl.* **2020**, *157*, 104746. [CrossRef]

11. Ji, W.; Xie, K.; Yan, S. Separation and recovery of heavy metals zinc and lead from phosphorus flue dust by vacuum metallurgy. *J. Environ. Manag.* **2021**, *294*, 113001. [CrossRef]
12. Li, Y.; Feng, H.X.; Wang, J.S.; She, X.F.; Wang, G.; Zuo, H.B.; Xue, Q.G. Current status of the technology for utilizing difficult-to-treat dust and sludge produced from the steel industry. *J. Clean. Prod.* **2022**, *367*, 132909. [CrossRef]
13. Lv, W.; Gan, M.; Fan, X.H.; Sun, Z.Q.; Zhang, R.C.; Ji, Z.Y.; Chen, X.L. Reaction Behavior and Transformation Path of Zinc in the Heating-Up Zone during Sintering Process. *Sustainability* **2022**, *14*, 10147. [CrossRef]
14. Wang, Y.N.; Gan, M.; Fan, X.H.; Lv, W.; Ji, Z.Y. Phase Transformation and Enhanced Zn Removal Technology During the Iron Ore Sintering Process. *JOM* **2022**, *75*, 310–320. [CrossRef]
15. Zhu, D.; Wang, D.; Pan, J.; Tian, H.; Xue, Y. A study on the zinc removal kinetics and mechanism of zinc-bearing dust pellets in direct reduction. *Powder Technol.* **2021**, *380*, 273–281. [CrossRef]
16. Luo, X.; Wang, C.; Shi, X.; Li, X.; Wei, C.; Li, M.; Deng, Z. Selective separation of zinc and iron/carbon from blast furnace dust via a hydrometallurgical cooperative leaching method. *Waste Manag.* **2022**, *139*, 116–123. [CrossRef]
17. Xue, Y.; Liu, X.; Zhang, N.; Guo, S.; Xie, Z.; Xu, C. A novel process for the treatment of steelmaking converter dust: Selective leaching and recovery of zinc sulfate and synthesis of iron oxides@HTCC photocatalysts by carbonizing carbohydrates. *Hydrometallurgy* **2023**, *217*, 106039. [CrossRef]
18. Bruckard, W.J.; Davey, K.J.; Rodopoulos, T.; Woodcock, J.T.; Italiano, J. Water leaching and magnetic separation for decreasing the chloride level and upgrading the zinc content of EAF steelmaking baghouse dusts. *Int. J. Miner. Process.* **2005**, *75*, 1–20. [CrossRef]
19. Kelebek, S.; Yörük, S.; Davis, B. Characterization of basic oxygen furnace dust and zinc removal by acid leaching. *Miner. Eng.* **2004**, *17*, 285–291. [CrossRef]
20. Oustadakis, P.; Tsakiridis, P.E.; Katsiapi, A.; Agatzini-Leonardou, S. Hydrometallurgical process for zinc recovery from electric arc furnace dust (EAFD): Part I: Characterization and leaching by diluted sulphuric acid. *J. Hazard. Mater.* **2010**, *179*, 1–7. [CrossRef]
21. Filippou, D.; Demopoulos, G.P. A Reaction Kinetic Model for the Leaching of Industrial Zinc Ferrite Particulates in Sulphuric Acid Media. *Can. Metall. Q.* **1992**, *31*, 41–54. [CrossRef]
22. Chairaksa-Fujimoto, R.; Maruyama, K.; Miki, T.; Nagasaka, T. The selective alkaline leaching of zinc oxide from Electric Arc Furnace dust pre-treated with calcium oxide. *Hydrometallurgy* **2016**, *159*, 120–125. [CrossRef]
23. Dutra, A.; Paiva, P.; Tavares, L.M. Alkaline leaching of zinc from electric arc furnace steel dust. *Miner. Eng.* **2006**, *19*, 478–485. [CrossRef]
24. Orhan, G. Leaching and cementation of heavy metals from electric arc furnace dust in alkaline medium. *Hydrometallurgy* **2005**, *78*, 236–245. [CrossRef]
25. Kashyap, V.; Taylor, P. Selective Extraction of Zinc from Zinc Ferrite. *Min. Metall. Explor.* **2021**, *38*, 27–36. [CrossRef]
26. Jaafar, I.; Griffiths, A.J.; Hopkins, A.C.; Steer, J.M.; Griffiths, M.H.; Sapsford, D.J. An evaluation of chlorination for the removal of zinc from steelmaking dusts. *Miner. Eng.* **2011**, *24*, 1028–1030. [CrossRef]
27. Omran, M.; Fabritius, T. Utilization of blast furnace sludge for the removal of zinc from steelmaking dusts using microwave heating. *Sep. Purif. Technol.* **2019**, *210*, 867–884. [CrossRef]
28. Gargul, K.; Boryczko, B. Removal of zinc from dusts and sludges from basic oxygen furnaces in the process of ammoniacal leaching. *Arch. Civ. Mech. Eng.* **2015**, *15*, 179–187. [CrossRef]
29. Lv, W.; Gan, M.; Fan, X.; Ji, Z.; Chen, X. Mechanism of calcium oxide promoting the separation of zinc and iron in metallurgical dust under reducing atmosphere. *J. Mater. Res. Technol.* **2019**, *8*, 5745–5752. [CrossRef]
30. Han, J.; Liu, W.; Qin, W.; Peng, B.; Yang, K.; Zheng, Y. Recovery of zinc and iron from high iron-bearing zinc calcine by selective reduction roasting. *J. Ind. Eng. Chem.* **2015**, *22*, 272–279. [CrossRef]
31. Xie, Z.Q.; Jiang, T.; Chen, F.; Guo, Y.F.; Wang, S.; Yang, L.Z. Phase Transformation and Zinc Extraction from Zinc Ferrite by Calcium Roasting and Ammonia Leaching Process. *Crystals* **2022**, *12*, 641. [CrossRef]

Disclaimer/Publisher's Note: The statements, opinions and data contained in all publications are solely those of the individual author(s) and contributor(s) and not of MDPI and/or the editor(s). MDPI and/or the editor(s) disclaim responsibility for any injury to people or property resulting from any ideas, methods, instructions or products referred to in the content.